Molecules and Cells

Cell Death-Associated Ribosomal RNA Cleavage in Postmortem Tissues and Its Forensic Applications

Ji Yeon Kim[1,2,4], Yunmi Kim[1,2,4], Hyo Kyeong Cha[1,2,4], Hye Young Lim[1,2], Hyungsub Kim[1], Sooyoung Chung[3], Juck-Joon Hwang[1], Seong Hwan Park[1], and Gi Hoon Son[1,2,*]

[1]Department of Legal Medicine, [2]Department of Biomedical Sciences, College of Medicine, Korea University, Seoul 02841, Korea, [3]Department of Brain and Cognitive Sciences, Scranton College, Ewha Womans University, Seoul 03760, Korea, [4]These authors contributed equally to this work.
*Correspondence: songh@korea.ac.kr
http://dx.doi.org/10.14348/molcells.2017.0039
www.molcells.org

Estimation of postmortem interval (PMI) is a key issue in the field of forensic pathology. With the availability of quantitative analysis of RNA levels in postmortem tissues, several studies have assessed the postmortem degradation of constitutively expressed RNA species to estimate PMI. However, conventional RNA quantification as well as biochemical and physiological changes employed thus far have limitations related to standardization or normalization. The present study focuses on an interesting feature of the subdomains of certain RNA species, in which they are site-specifically cleaved during apoptotic cell death. We found that the D8 divergent domain of ribosomal RNA (rRNA) bearing cell death-related cleavage sites was rapidly removed during postmortem RNA degradation. In contrast to the fragile domain, the 5′ terminal region of 28S rRNA was remarkably stable during the postmortem period. Importantly, the differences in the degradation rates between the two domains in mammalian 28S rRNA were highly proportional to increasing PMI with a significant linear correlation observed in mice as well as human autopsy tissues. In conclusion, we demonstrate that comparison of the degradation rates between domains of a single RNA species provides quantitative information on postmortem degradation states, which can be applied for the estimation of PMI.

Keywords: 28S ribosomal RNA (rRNA), cell death-associated RNA cleavage, postmortem interval (PMI), RNA degradation

INTRODUCTION

The accurate estimation of postmortem interval (PMI) is critical to criminal investigations in the field of forensic science. A wide spectrum of methods has been developed and tested to estimate the time of death. For example, several physical, pathophysiological, biochemical, and microbiological processes occurring during the postmortem period have been proposed for PMI estimation (Henssge and Madea, 2007; Smart and Kaliszan, 2012). However, these assessment methods are still largely unreliable and inaccurate because of their susceptibility to environmental factors as well as large variations that exist among individuals. Furthermore, these methods are applicable with sufficient accuracy to limited periods within a day. Although entomological evidence is often utilized to estimate PMI for longer periods, such indirect approaches are more profoundly influenced by uncontrollable environmental factors (Goff, 1993). Therefore, the standardized evaluation of parameters that change constantly with time after death is a prerequisite for an accurate estimation of PMI.

Received 16 March, 2017; revised 24 April, 2017; accepted 12 May, 2017; published online 15 June, 2017

eISSN: 0219-1032
© The Korean Society for Molecular and Cellular Biology. All rights reserved.
This is an open-access article distributed under the terms of the Creative Commons Attribution-NonCommercial-ShareAlike 3.0 Unported License. To view a copy of this license, visit http://creativecommons.org/licenses/by-nc-sa/3.0/.

With advances in molecular biology, novel approaches based on macromolecules such as nucleic acids have been recently developed for a wide range of forensic pathology analyses. For example, several studies demonstrate that RNA analysis can be valuable for identifying body fluid, estimating wound age, and diagnosing the cause/mode of death (Bauer, 2007; Maeda et al., 2014; Vennemann and Koppelkam, 2010a). In this context, several studies have proposed that time-dependent decay of RNA during the postmortem period can be utilized as a possible indicator for PMI estimation, since RNA degradation or loss of certain RNA transcripts after organismal death occurs rapidly and in a time-dependent manner (Bauer et al., 2003; Li et al., 2014; Lv et al., 2016; Poór et al., 2016; Sampaio-Silva et al., 2013). Multiple classes of RNA species such as messenger RNAs (mRNAs), ribosomal RNAs (rRNAs), and microRNAs have been tested for this purpose. However, correlating the degradation of RNA species with PMI still remains an area of concern, primarily owing to difficulties in the standardization and/or normalization of quantitative analyses with sufficient accuracy and reproducibility (Vennemann and Koppelkamm 2010a; 2010b). Postmortem RNA profiles represent preexisting pathophysiological states along with postmortem conditions, thereby leading to large variations among individuals. Furthermore, the differential kinetics of decay among different classes of RNA species and even among mRNA transcripts from different genes also impedes precise and quantitative measurement of RNA levels from postmortem tissues (Chung et al., 2012; Lv et al., 2016; Sobue et al., 2016).

It is noteworthy that certain RNA molecules, particularly rRNAs, are cleaved into several distinct fragments during apoptotic cell death (Degen et al., 2000b). For example, 28S rRNA has been reported to undergo distinct fragmentation during apoptotic cell death, and subsequent studies have mapped the cleavage sites (Houge et al., 1993; 1995). Considering that extensive cell death processes accompanying organismal death, the present study aims to examine whether postmortem changes in cell death-associated RNA cleavage in a fragile domain compared to a relatively stable domain can be used to estimate PMI. It is possible that, compared to conventional methods (i.e., comparison between targets and internal controls), the intramolecular comparison between domains with differential degradation rates will provide more reliable indices for RNA-based PMI estimation. Therefore, 28S rRNA could be an excellent model because its secondary structure and cleavage sites in divergent domains are well defined.

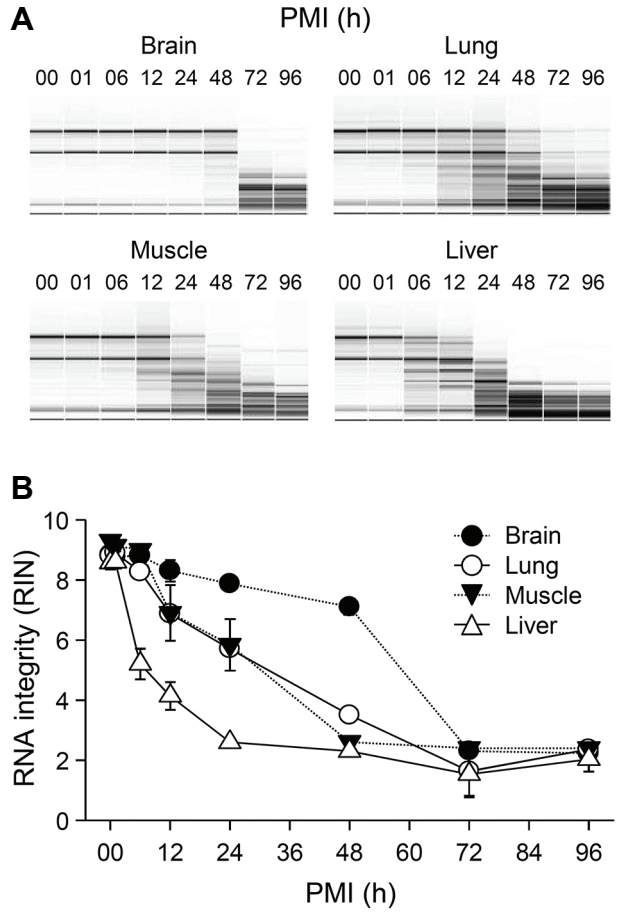

Fig. 1. Changes in RNA integrity in postmortem mouse tissues. (A) Degradation profiles of total RNA samples isolated from brain, lung, muscle, and liver tissues are examined at different postmortem periods by RNA electropherogram. (B) RNA integrity numbers (RINs) are plotted by postmortem interval (PMI) and expressed as mean ± SE (n = 3).

MATERIALS AND METHODS

Preparation tissues

In the animal experiments shown in Figs. 1, 2, and 3, male C57BL/6J mice at the age of 10 weeks were euthanized by isoflurane anesthesia followed by cervical dislocation. The mice corpses were then maintained at room temperature (21-23℃) for 0, 1, 6, 12, 24, 48, 72, and 96 h. The brain (cerebral cortex), lung, muscle (quadriceps femoris), and liver were isolated at the indicated postmortem period and frozen immediately in liquid nitrogen. In the experiments shown in Fig. 4, four male mice were sacrificed and then the cerebral cortex and liver were immediately isolated from each animal. Nineteen pieces of tissues per animal were prepared, divided into multi-well plates, and incubated at room temperature for up to 72 h. Samples were collected every 4 h, and immediately frozen in liquid nitrogen. Use of animals and related experimental procedures were approved by the Institutional Animal Care and Use Committee of Korea University (KU-IACUC). For human tissues used in Fig. 5, brain (occipital lobe of the cerebral cortex) and liver autopsy tissues of two subjects were collected from selected medicolegal autopsy cases with help from the National Forensic Service (NFS) of Korea. Dissected tissues were divided into pieces with similar sizes (30-50 mg each) and further maintained at room temperature for 36 h. Incubated human autopsy tissues were collected every 4 h, immediately frozen in liquid nitrogen, and then stored at −80℃ until RNA extraction.

RNA isolation and quantitative reverse transcription-polymerase chain reaction (qRT-PCR)

RNA isolation and qRT-PCR analyses were carried out as previously described with few modifications (Chung et al., 2012; Son et al., 2014). Tissues were homogenized in Trizol™ reagent and total RNA were isolated using miRNeasy Mini Kit (Qiagen, Germany) according to the manufacturer's instructions. RNA concentration and integrity were assessed using the NanoDrop 2000 (NanoDrop Technologies, USA) and Agilent 2100 Bioanalyzer, which calculates RNA integrity number (RIN) values of assayed RNA samples (Agilent Technologies, USA). For qRT-PCR, 500 ng of each total RNA sample was reverse-transcribed using MMLV reverse transcriptase (Promega, USA) by using the random priming method. Then, aliquots of cDNA were subjected to quantitative real-time PCR in the presence of SYBR Green I (Thermo Fisher Scientific, USA). Primer sequences used for real-time qRT-PCR were as follows: human/mouse 28S rRNA 5′ terminal upper, 5′-CCT CAG ATC AGA CGT GGC GA-3′; human/mouse 28S rRNA 5′ terminal lower, 5′-CTG GGC TCT TCC CTG TTC AC-3′; mouse 28S rRNA D8 upper, 5′-CAT CGC CTC TCC CGA GGT GCG TG-3′; mouse 28S rRNA D8 lower, 5′-GTT CTA AGT CGG CTG CTA GGC-3′; human 28S rRNA D8 upper, 5′-CCC CCG GGG CCG CGG TTC CG-3′; and human 28S rRNA D8 lower, 5′-CAG TTC TAA GTC GGC TGC TAG G-3′.

Data analysis

All qRT-PCR reactions were conducted in duplicate, and the average Ct values were used for accompanying analyses. ΔCt values (defined as $\Delta Ct = Ct - Ct_{t=0}$) were used to represent the relative amount of an RNA fragment of interest. Pooled RNA samples obtained at 0 h and fresh RNA isolated from cultured HeLa cells were used as references for mice and human specimens, respectively. The ratio between different domains of 28S rRNA was calculated by $2^{-\Delta\Delta Ct}$ method. The p values of the statistical significance were examined by linear regression accompanied by Pearson's correlation. Statistical significance was set at $p < 0.05$.

RESULTS

Postmortem RNA decay in various murine tissues

Despite the unexpectedly high stability of RNA in certain conditions (Bahar et al., 2007; Heinrich et al., 2007), it is widely accepted that RNA undergoes postmortem degradation by endogenous RNase activities as well as environmental causes including microbiological contamination. Previous studies proposed the potential application of time- and tissue-dependent RNA decay to estimate PMI (Bauer et al., 2003; Li et al., 2014; Lv et al., 2016; Poór et al., 2016; Sampaio-Silva et al., 2013). Therefore, we initially examined the loss of RNA integrity in four tissues of interest isolated from mice corpses maintained for the indicated postmortem period. For RNA quality assessment, we determined the RNA integrity number (RIN) that represents the integrity of the RNA samples from electropherograms (Fig. 1A). Loss of RNA during the postmortem period was observed in all tested tissues, but the extent of degradation denoted tissue specificity. RNA extracted from brain tissue was relatively stable during the postmortem period and showed RIN values over 6.0 up to 48 h, while hepatic RNA was rapidly degraded and the RIN values were less than 4.0 within 24 h (Fig. 1B). RNA samples from lung or muscle tissues exhibited intermediate rates of degradation. As a result, linear phases of RNA decay were different from each other from 12 to 72 h of PMI in a tissue dependent manner. It is also noteworthy that RIN values from all examined tissues reached to approximately 2.0 by 72 h and remained unchanged up to 96 h, suggesting that the correlation between RNA degradation and PMI may be suitable for estimation of PMI ranging from 1 to 3 days.

Differential degradation rate between the subdomains of mouse 28S rRNA

Next, we examined the PMI-dependent degradation of 28S rRNA that is the most abundant and constitutively expressed RNA species in living cells, and is highly conserved in nucleotide sequences and secondary structure among different mammalian species. Within the murine 28S rRNA transcript, we mainly focused on the 5′ terminal stable regions associating with 5.8S rRNA and the D8 divergent domain harboring cell death-associated cleavage sites, which are well conserved among mouse, rat and human (Fig. 2A; Houge et al., 1995). When we compared the relative abundance of these two subdomains, as measured by -ΔCt values from the beginning by qRT-PCR, the relative levels of the 5′ terminal regions were barely reduced in all examined tissues (Figs. 2B-2E, closed circles). By contrast, -ΔCt values for the D8 domain as a PCR amplicon gradually decreased with PMI, and the degradation rates of this region among tissues were comparable to the extent to which the RIN values decreased during the postmortem period (Figs. 2B-2E, open circles). As a result, differences in relative abundance between these two regions (i.e. areas between curves) were increased up to 96 h of PMI. Based on these findings, we then plotted the changes in the expression levels of the D8 domains relative to the 5′ terminal region of 28S rRNA against PMI. Notably, logarithmic transformation of the D8 domain-to-5′ terminal region ratio exhibited significant linear correlations with PMI, as measured by the Pearson's correlation test, in all examined tissues (Fig. 3; $r < -0.5$ and $p < 0.01$ for all examined tissues). Slopes of linear regression show that the ratio between the two subdomains rapidly decreased in the liver, but decreased slowly in the brain. This was similar to the overall RNA decay rates as shown above by RIN values.

We then examined whether differential degradation rates between the 5′ terminal region and D8 domains of 28S rRNA can be found in mice tissues maintained *ex vivo* and collected at 4-h intervals, in order to develop a practical method applicable to human autopsy tissues. For this purpose, brain and liver tissues were mainly examined because RNA extracted from brain tissue was the most stable, and hepatic RNA was the most rapidly degraded sample among the examined tissues. In both tissues, the relative amounts of 5′ terminal region 28S rRNA were relatively stable and maintained for up to 72 h, whereas the D8 domain successively disappeared with PMI (Figs. 4A and 4B). Similarly with the

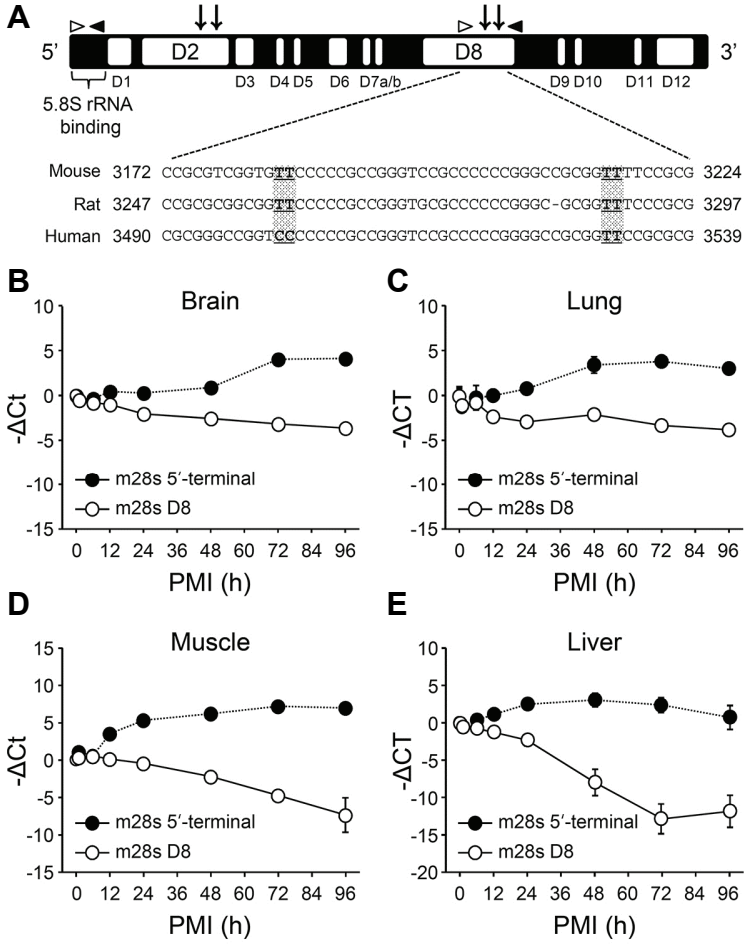

Fig. 2. Differential degradation rates between mouse 28S rRNA subregions in mouse corpses. (A) A Schematic representation of mammalian 28S rRNA. Divergent domains are shown as white boxes. 28S rRNA binds to 5.8S rRNA through its 5′ terminal regions. Arrows on the D2 and D8 domains indicate cell death-associated cleavage sites and arrowheads indicate primer-binding sites. Conserved cell death-associated cleavage sequences in the D8 domains among mouse, rat and human 28S rRNA are also shown below. (B-E) Postmortem changes in ΔCt values (ΔCt = Ct - $Ct_{t=0}$) representing the relative amounts of 5′ terminal region (closed circle) and D8 domain (open circle) of 28S rRNA in the brain (B), lung (C), muscle (D), and liver (E) tissues from mouse corpses maintained for the indicated postmortem period. Data are expressed as mean ± SE (n = 3).

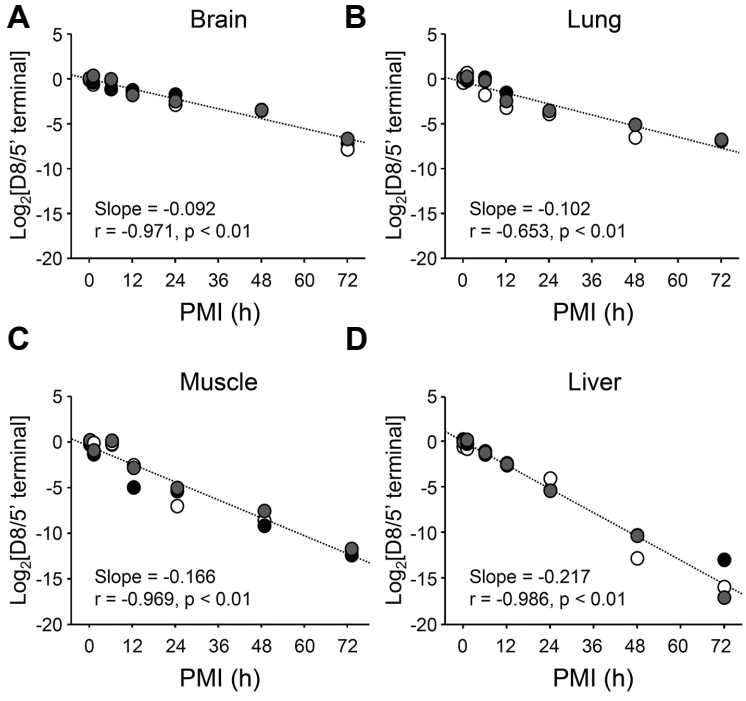

Fig. 3. Postmortem changes in the D8 domain-to-5′ terminal region ratio. The amount of D8 domains relative to 5′ terminal region of mouse 28S rRNA are examined in the brain (A), lung (B), muscle (C), and liver (D) tissues from mouse corpses. Experiments were carried out three times and the results are plotted by PMI and statistically evaluated by Pearson's correlation.

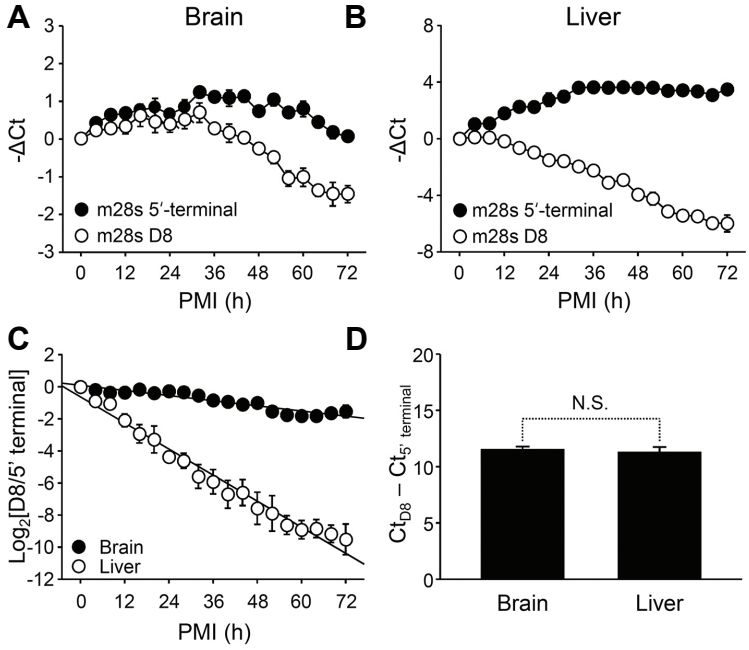

Fig. 4. Differential degradation rates between mouse 28S rRNA subregions in isolated mouse tissues incubated *ex vivo*. (A, B) Postmortem changes in ΔCt values (ΔCt = Ct - $Ct_{t=0}$) representing the relative amounts of 5′ terminal region (closed circle) and D8 domain (open circle) of mouse 28S rRNA in the brain (A) and liver (B) tissues incubated *ex vivo* for the indicated period. (C) Amount of D8 domains relative to 5′ terminal region of mouse 28S ribosomal RNA in the brain (closed) and liver (open) tissues are plotted by PMI and statistically evaluated by Pearson's correlation (Slope = -0.037, r = -0.831, $p < 0.01$ for brain and Slope = -0.146, r = -0.921, $p < 0.01$ for liver). (D) Differences between Ct values of the D8 domains and 5′ terminal region (i.e. Ct_{D8} - $Ct_{5'\text{-terminal}}$) are examined in fresh brain and liver tissues. Data are expressed as mean ± SE (n = 3 for (A-C) and n = 7 for (D)).

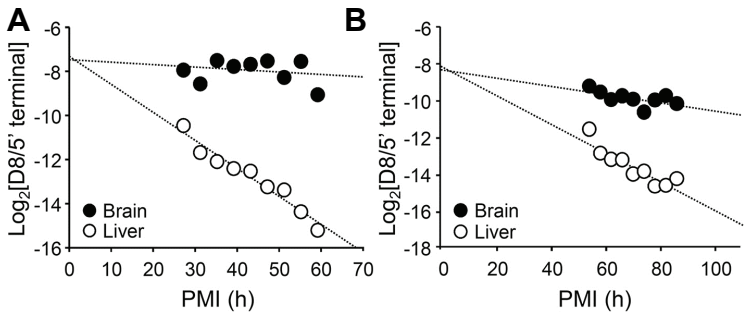

Fig. 5. Postmortem changes in the D8 domain-to-5′ terminal region ratio in human autopsy tissues. (A, B) The amount of D8 domains relative to 5′ terminal region of mouse 28S rRNA are examined in the human brain (closed) and liver (open) tissues incubated *ex vivo* for the indicated period. Amount of D8 domains relative to 5′ terminal region of mouse 28S ribosomal RNA in the brain (closed) and liver (open) tissues are plotted by PMI and statistically evaluated by Pearson's correlation (A: Slope = -0.011, r = 0.226, p = 0.559 for brain and Slope = -0.127, r = -0.976, $p < 0.01$ for liver; B: Slope = -0.022, r = -0.615, p = 0.078 for brain and Slope = -0.080, r = -0.904, $p < 0.01$ for liver). Actual time-of-death for each case were set at 0 h. Tissues were isolated and then subjected to *ex vivo* incubation from 27 (A)

results from mice corpses, the D8 domain showed more rapid reduction in the liver than in the brain tissues incubated *ex vivo*. The same logarithmic transformation of the D8 domain-to-5′ terminal region ratio described above also resulted in significant linear correlation with PMI in tissues maintained *ex vivo* (Fig. 4C; $p < 2.20E\text{-}16$ for both tissues by Pearson's correlation). We then examined the D8 domain-to-5′ terminal region ratio represented by differences in the Ct values of two domains in the fresh tissues. The D8-to-5′ terminal ratios in fresh brain and liver tissues were not significantly different, demonstrating that the steady-state values in living cells are essentially the same in both tissues (Fig. 4D). Our findings clearly demonstrate that different domains of a single RNA species exhibit differential degradation rates during the postmortem period, and the extent of differences in remaining amounts of the RNA regions postmortem can be transformed to a linear model against PMI.

Estimation of PMI in human autopsy cases: a proof-of-concept study

Finally, we tested our method to estimate PMI in human cases as a proof-of-concept study. We maintained the brain and liver autopsy tissues *ex vivo* at room temperature and prepared RNA samples from aliquots of tissues at 4-h intervals. Autopsy tissues were quickly prepared and then subjected to successive collections from 27 h (Fig. 5A) and 54 h (Fig. 5B) postmortem, respectively. Similar to our observations in mouse tissues, faster degradation of the D8 regions

than the 5′ terminal regions of human 28S rRNA was already observed at the beginning of the *ex vivo* incubation. Moreover, the ratios of D8 domain-to-5′-terminal region in liver tissues decreased faster than those obtained from the brain tissues in both cases. Based on the above finding that D8-to-5′ terminal ratios for both tissues are similar at the time of death (Fig. 4D), we considered the time when two lines made by extrapolation of the results meet as an estimated time-of-death. The differences between the actual and estimated time-of-death were +1.29 h (4.70% for error rate) for the first case and +6.98 (12.96%) for the second. These findings collectively suggest that differences between stable and fragile domains of the human 28S rRNA exhibit a linear and significant correlation against the PMI with a characteristic slope in a given tissue and the comparison of multiple tissues can be used to estimate the PMI.

DISCUSSION

The present study describes a novel method to estimate PMI by comparing differentially degrading domains of a single RNA species in postmortem tissues. Because substantial degradation of RNA species in postmortem tissues by physical, chemical, and enzymatic mechanisms was highlighted, degradation profiles of RNA were suggested as a valuable tool for PMI estimation. Thus, the quantitative and accurate analysis of the extent to which RNA degrade postmortem garnered much research interest, and several elegant methods have been proposed to date.

Although different classes of RNA species such as rRNAs, mRNAs, and small RNAs have been extensively tested, PMI estimation based on RNA degradation is still highly debatable for the following reasons. First, most studies to date are based on constitutively expressed but RNA polymerase II (RNA Pol II)-dependent RNA species, such as mRNA transcripts of house-keeping genes and several miRNAs. RNA Pol II-dependent gene transcription is profoundly influenced by antemortem factors as well as postmortem situations, thus leading to large variations among individuals (Rienzo and Casamassimi, 2016; Zhang et al., 2016). Furthermore, standardization of postmortem RNA degradation profiles is important because different RNA transcripts show different degradation kinetics and steady-state expression levels among individuals, and even the overall RNA extraction efficacy is altered with PMI (González-Herrera et al., 2013; Koppelkamm et al., 2010); therefore, it is difficult to standardize or normalize the extent of RNA degradation in a quantitative manner. Despite the development of mathematical models, it is difficult to correlate RNA integrity with PMI because degradation profiles of certain RNA transcript and changes in overall RNA integrity exhibit linear correlations within limited postmortem periods. Therefore, it can be postulated that alternative approaches other than conventional quantification methods are required for RNA-based PMI estimation.

To overcome the limitations described above, the present study proposes a novel method for PMI estimation by comparing two domains of a single RNA species that show differential degradation rates. We employed 28S rRNA as a model because it is the most abundant RNA species, and its transcription by RNA Pol I is less affected by antemortem conditions, thereby barely exhibiting individual variations compared to gene transcripts produced by RNA Pol II (Zhang et al., 2016). Furthermore, its secondary structure (Gorski et al., 1987; Michot et al., 1984) as well as the domains that are vulnerable to cell death-associated cleavage are well defined (Houge et al., 1993; 1995). Therefore, we compared relative amounts of two 28S rRNA domains and then correlated them with PMI. The 5′ terminal region and D8 domain of the 28S rRNA were selected as stable and fragile domains, respectively. As shown in Fig. 2, the 5′ terminal region of the 28S rRNA was highly stable in all tested postmortem tissues up to 4 days. This exceptional stability of the domain is probably because of its secondary and tertiary structure; the domain forms tight stem-like structures by intramolecular base-pairing, and further associates with the 5.8S rRNA subunit (Houge et al., 1995; Michot et al., 1982; Walker et al., 1982). It is most plausible that such structural features confer remarkable stability to the domain during postmortem degradation. In contrast, 28S rRNA consists of various divergent domains (denoted as D1 to D12) (Michot et al., 1984), and some of these divergent domains were shown to be rapidly and specifically cleaved in apoptotic cells. Among the divergent domains, the two largest divergent domains, D2 and D8, are highly vulnerable to cell death-associated 28S rRNA cleavage. In particular, the D8 domain contains multiple cleavage sites that can be recognized by cell death-activated RNases and caspases, and thus appears to be the most susceptible region for cell death-associated degradation (Degen et al., 2000b; Houge et al., 1995; Nadano and Sato, 2000; Naito et al., 2009). Considering that massive cell death accompanies systemic death during the postmortem period (Maeda et al., 2010), it is likely that the D8 domain of the 28S rRNA is rapidly removed in postmortem tissues in contrast to the stable 5′ terminal region.

Substantial changes in the ratio of D8-to-5′ terminal regions showed a significant and linear correlation with PMI, at least up to 3 days, with characteristic slopes depending on examined tissue types in tissues isolated and maintained *ex vivo* as well as mice corpses (Figs. 3 and 4). The slopes deduced by linear regression analysis on different tissues highly correlated with postmortem changes in RIN values, indicating that they may represent overall RNase activity in the given tissue types. Since the steady-state D8-to-5′ terminal ratio in living cells was essentially the same in brain and liver tissue (Fig. 4D), the time-of-death could be estimated by calculating the time when two extrapolated lines obtained from brain and liver tissues incubated *ex vivo* meet. Indeed, the predicted time-of-death was close to the real value in human autopsy tissues (Fig. 5), demonstrating that the proposed method can provide a more convenient and relatively accurate tool to estimate PMI. However, it still remains elusive how slopes calculated by linear regression of the results obtained in human autopsy tissues incubated *ex vivo* can be adjusted for practical applications in human autopsy cases with improved accuracy, as there are some differences in the decreasing rates of the D8-to-5′ terminal ratio between tissues maintained *ex vivo* and in mouse corpses. Environmental factors such as temperature and humidity may also influ-

ence the rates. Further analyses on sufficient numbers of autopsy cases and development of multiple target RNA species in addition to 28S rRNA may provide a mathematical model for improving the accuracy of the present proof-of-concept study.

In addition to 28S rRNA as exemplified in the present study, several RNA species were also found to be cleaved in association with cell death processes. It is reasonable to expect that comparing multiple indices would be greatly helpful for precise PMI estimation. For example, RNase L, an inducible endonuclease, was initially identified as a mediator of type 1 interferon-induced antiviral activity and has diverse cellular roles in the regulation of cell proliferation, senescence, and apoptosis. Although RNase L was originally shown to mediate the endonucleolytic cleavage of both viral and rRNAs, more recent evidence indicate that RNase L also functions in the regulation of cellular mRNAs as an important mechanism mediating its diverse biological functions (Brennan-Laun et al., 2014; Naito et al., 2009). As RNase L usually exerts site-specific nucleolytic activity, target sites of RNase L on housekeeping mRNA species can be used for PMI estimation similar to 28S rRNA. It is also noteworthy that some small RNAs constituting small nuclear ribonucleoproteins (snRNPs) undergo site-specific and cell death-related cleavage (Degen et al., 2000b). U1 snRNA, a component of U1 snRNP mediating pre-mRNA splicing and hY RNAs constituting Ro RNP complex are well-known examples. Interestingly, related members such as U2, U3, U4, U5, and U6 snRNAs were not subjected to RNA modifications during cell death, suggesting that they can be used as stable targets similar to the 5′ terminal domain of the 28S rRNA. The unusual cleavage/degradation of these small RNAs is dependent on the activation of caspases as well as induced RNase activity, indicating that caspase-activated RNases may be responsible for the processes (Degen et al., 2000a; Rutjes et al., 1999).

It is also noteworthy that massive cellular death may occur several hours to even several days after systemic or organismal death (Maeda et al., 2010). In this regard, 28S rRNA cleavage profiles also provide interesting information on cellular events during the early phase of the postmortem period in addition to the implications in PMI estimation as discussed thus far. First, *de novo* RNA synthesis may persist longer than expected, as the stable region of 28S rRNA accumulates for 48 h in the hepatic tissue and even up to 96 h in the brain (Figs. 2 and 4). Furthermore, cell death-associated 28S rRNA degradation in the postmortem brain tissues showed a delayed initiation compared with the liver tissues (Figs. 4A and 4B). The observation strongly suggests that postmortem RNA expression and degradation profiles can be profoundly influenced by cell type-specific properties related to supravital responses. It is most likely that differential changes in the ratio of D8-to-5′ terminal regions among tissues collectively represent postmortem viability or susceptibility to hypoxic conditions of given tissues or cell types as well as composition and abundance of RNA degrading enzymes. This notion also implies that such cell type-dependent features impacting RNA profiles in both quantitative and qualitative manners should be considered in postmortem RNA analyses along with pathophysiological causes programing antemortem RNA expression.

Taken together, the present study proposes a novel tool for PMI estimation based on cell death-associated RNA cleavage. Despite the practical issues presented for future investigation, the proposed method has several advantages compared to the previous conventional approaches. First, our approach utilizes the intramolecular comparison of well-defined domains from the single RNA transcript, thus free from errors and variations produced by comparing the expression levels of multiple distinct RNA species for normalization. Subregions originating from a single RNA transcript are produced at the same amount, and the steady-state ratio is well maintained at the equilibrium, particularly in the case of constitutively expressed genes such as 28S rRNA. Second, by combining *ex vivo* incubation as exemplified in the present study, and also by comparing multiple tissues, our method provides a more convenient procedure that is compatible with simplified mathematical modeling. It is also noteworthy that postmortem gene expression profiling at a genome-wide level is emerging in the area of forensic science for the examination of the causes and modes of death or for identification of tissues/body fluids. To ensure reliable results, PMI, tissue pH, and/or RIN values are currently considered for evaluating the quality and integrity of the postmortem RNA samples (Sobue et al., 2016). The extent of the cell death-associated RNA cleavage would also provide realistic information on the quality of RNA samples prepared from postmortem tissues with different ante- and postmortem conditions.

ACKNOWLEDGEMENTS

This work was supported by the Korean Ministry of Science, ICT, and Future Planning through the National Research Foundation of Korea (NRF-2012M3A9C7050135, NRF-2015 M3A9E7029176, NRF-2016M3C7A1904340); the Korean National Police Agency through the Research and Development of Police Science and Technology project (PA-G000001/2016-401); and the Korea University grant program (K1422401). J. Y. Kim, Y. Kim and H. K. Cha were supported by the Brain Korea 21 PLUS program. Editage edited the manuscript.

REFERENCES

Bahar, B., Monahan, F.J., Moloney, A.P., Schmidt, O., MacHugh, D.E., and Sweeney, T. (2007). Long-term stability of RNA in post-mortem bovine skeletal muscle, liver and subcutaneous adipose tissues. BMC Mol. Biol. *8*, 108-120.

Bauer, M. (2007). RNA in forensic science. Forensic Sci. Int. Genet. *1*, 69-74.

Bauer, M., Gramlich, I., Polzin, S., and Patzelt, D. (2003). Quantification of mRNA degradation as possible indicator of postmortem interval-a pilot study. Leg. Med. *5*, 220-227.

Brennan-Laun, S.E., Ezelle, H.J., Li, X.L., and Hassel, B.A. (2014). RNase-L control of cellular mRNAs: roles in biologic functions and mechanisms of substrate targeting. J. Interferon Cytokine Res. *34*, 275-288.

Chung, U., Seo, J.S., Kim, Y.H., Son, G.H., and Hwang, J.J. (2012).

Quantitative analyses of postmortem heat shock protein mRNA profiles in the occipital lobes of human cerebral cortices: implications in cause of death. Mol. Cells *34*, 473-480.

Degen, W.G., Aarssen, Y., Pruijn, G.J., Utz, P.J., and Venrooij, W.J. (2000a). The fate of U1 snRNP during anti-Fas induced apoptosis: specific cleavage of the U1 snRNA molecule. Cell Death Differ. *7*, 70-79.

Degen, W.G., Pruijn, G.J., Raats, J.M., and Venrooij, W.J. (2000b). Caspase-dependent cleavage of nucleic acids. Cell Death Differ. *7*, 616-627.

Goff, M.L. (1993). Estimation of postmortem interval using arthropod development and successional patterns. Forensic. Sci. Rev. *5*, 81-94.

González-Herrera, L., Valenzuela, A., Marchal, J.A., Lorente, J.A., and Villanueva, E. (2013). Studies on RNA integrity and gene expression in human myocardial tissue, pericardial fluid and blood, and its postmortem stability. Forensic. Sci. Int. *232*, 218-228.

Gorski, J.L., Gonzalez, I.L., and Schmickel, R.D. (1987). The secondary structure of human 28S rRNA: the structure and evolution of a mosaic rRNA gene. J. Mol. Evol. 24, 236-251.

Heinrich, M., Matt, K., Lutz-Bonengel, S., and Schmidt, U. (2007). Successful RNA extraction from various human postmortem tissues. Int. J. Leg. Med. *121*, 136-142.

Henssge, C., and Madea, B. (2007). Estimation of the time since death. Forensic. Sci. Int. *165*, 182-184.

Houge, G., Døskeland, S.O., Bøe, E., and Lanotte, M. (1993). Selective cleavage of 28S rRNA variable regions V3 and V13 in myeloid leukemia cell apoptosis. FEBS Lett. *315*, 16-20.

Houge, G., Robaye, B., Eikhom, T.S., Golstein, J., Mellgren, G., Gjertsen, B.T., Lanotte, M., and Døskeland, S.O. (1995). Fine mapping of 28S rRNA sites specifically cleaved in cells undergoing apoptosis. Mol. Cell. Biol. *15*, 2051-2062.

Koppelkamm, A., Vennemann, B., Fracasso, T., Lutz-Bonengel, S., Schmidt, U., and Heinrich, M. (2010). Validation of adequate endogenous reference genes for the normalisation of qPCR gene expression data in human post mortem tissue. Int. J. Leg. Med. *124*, 371-380.

Li, W.C., Ma, K.J., Lv, Y.H., Zhang, P., Pan, H., Zhang, H., Wang, H.J., Ma, D., and Chen, L. (2014). Postmortem interval determination using 18S-rRNA and microRNA. Sci. Justice *54*, 307-310.

Lv, Y.H., Ma, J.L., Pan, H., Zhang, H., Li, W.C., Xue, A.M., Wang, H.J., Ma, K.J., and Chen, L. (2016). RNA degradation as described by a mathematical model for postmortem interval determination. J. Forensic. Leg. Med. *44*, 43-52.

Maeda, H., Zhu, B.L., Ishikawa, T., and Michiue, T. (2010) Forensic molecular pathology of violent deaths. Forensic Sci. Int. *203*, 83-92.

Maeda, H., Ishikawa, T., and Michiue, T. (2014). Forensic molecular pathology: its impacts on routine work, education and training. Leg. Med. (Tokyo) *16*, 61-69.

Michot, B., Bachellerie, J.P., and Raynal, F. (1982). Sequence and secondary structure of mouse 28S rRNA 5' terminal domain. Organisation of the 5.8S-28S rRNA complex. Nucleic Acids Res. *10*, 5273-5283.

Michot, B., Hassouna, N., and Bachellerie, J.P. (1984). Secondary structure of mouse 28S rRNA and general model for the folding of the large rRNA in eukaryotes. Nucleic Acids Res. *12*, 4259-4279.

Nadano, D., and Sato, T.A. (2000). Caspase-3-dependent and -independent degradation of 28S ribosomal RNA may be involved in the inhibition of protein synthesis during apoptosis initiated by death receptor engagement. J. Biol. Chem. *275*, 13967-13973.

Naito, T., Yokogawa, T., Takatori, S., Goda, K., Hiramoto, A., Sato, A., Kitade, Y., Sasaki, T., Matsuda, A., Fukushima, M., et al. (2009). Role of RNase L in apoptosis induced by 1-(3-C-ethynyl-beta-D-ribo-pentofuranosyl)cytosine. Cancer Che-mother. Pharmacol. *63*, 837-850.

Poór, V.S., Lukács, D., Nagy, T., Rácz, E., and Sipos, K. (2016). The rate of RNA degradation in human dental pulp reveals post-mortem interval. Int. J. Legal Med. *130*, 615-619.

Rienzo, M., and Casamassimi, A. (2016). Integrator complex and transcription regulation: Recent findings and pathophysiology. Biochim. Biophys. Acta *1859*, 1269-1280.

Rutjes, S.A., van der Heijden, A., Utz, P.J., van Venrooij, W.J., and Pruijn, G.J. (1999). Rapid nucleolytic degradation of the small cytoplasmic Y RNAs during apoptosis. J. Biol. Chem. *274*, 24799-24807.

Sampaio-Silva, F., Magalhães, T., Carvalho, F., Dinis-Oliveira, R.J., and Silvestre, R. (2013). Profiling of RNA degradation for estimation of post mortem interval. PLoS One *8*, e56507.

Smart, J.L., and Kaliszan, M. (2012). The post mortem temperature plateau and its role in the estimation of time of death. A review. Leg. Med. (Tokyo) *14*, 55-62.

Sobue, S., Sakata, K., Sekijima, Y., Qiao, S., Murate, T., and Ichihara, M. (2016). Characterization of gene expression profiling of mouse tissues obtained during the postmortem interval. Exp. Mol. Pathol. *100*, 482-492.

Son, G.H., Park, S.H., Kim, Y., Kim, J.Y., Kim, J.W., Chung, S., Kim, Y.H., Kim, H., Hwang, J.J., and Seo, J.S. (2014). Postmortem mRNA expression patterns in left ventricular myocardial tissues and their implications for forensic diagnosis of sudden cardiac death. Mol. Cells *37*, 241-247.

Vennemann, M., and Koppelkamm, A. (2010a). mRNA profiling in forensic genetics I: Possibilities and limitations. Forensic. Sci. Int. *203*, 71-75.

Vennemann, M., and Koppelkamm, A. (2010b). Postmortem mRNA profiling II: Practical considerations. Forensic. Sci. Int. *203*, 76-82.

Walker, T.A., Johnson, K.D., Olsen, G.J., Peters, M.A., and Pace, N.R. (1982). Enzymatic and chemical structure mapping of mouse 28S ribosomal ribonucleic acid contacts in 5.8S ribosomal ribonucleic acid. Biochemistry *21*, 2320-2329.

Zhang, Y., Najmi, S.M., and Schneider, D.A. (2016). Transcription factors that influence RNA polymerases I and II: To what extent is mechanism of action conserved? Biochim. Biophys. Acta *1860*, 246-255.